High-pressure effects on structural, magnetic, and vibrational properties of van der Waals antiferromagnet MnPS

Kozlenko, Denis; Lis, O; Dang, N.T.; Coak, Matt; Park, Je-Geun; Lukin, E.V.; Kichanov, S.E.; Golosova, N.O.; Zel, I.Yu.; Savenko, B.N.

DOI:
10.1103/PhysRevMaterials.8.024402

High-pressure effects on structural, magnetic, and vibrational properties of van der Waals antiferromagnet $MnPS_3$

D. P. Kozlenko,[1,*] O. N. Lis,[1,2] N. T. Dang,[3,4] M. Coak,[5,6,7] J.-G. Park,[6,7,8] E. V. Lukin,[1] S. E. Kichanov,[1] N. O. Golosova,[1] I. Yu. Zel,[1] and B. N. Savenko[1]

[1]*Frank Laboratory of Neutron Physics, JINR, 141980 Dubna, Moscow Region, Russian Federation*
[2]*Kazan Federal University, 420008, Kazan, Russian Federation*
[3]*Institute of Research and Development, Duy Tan University, 550000 Danang, Vietnam*
[4]*Faculty of Environmental and Natural Sciences, Duy Tan University, 550000 Danang, Vietnam*
[5]*School of Physics and Astronomy, University of Birmingham, Edgbaston, Birmingham B15 2TT, United Kingdom*
[6]*Center for Correlated Electron Systems, Institute for Basic Science, Seoul 08826, Republic of Korea*
[7]*Department of Physics and Astronomy, Seoul National University, Seoul 08826, Republic of Korea*
[8]*Center for Quantum Materials, Seoul National University, Seoul 08826, Republic of Korea*

(Received 17 November 2023; accepted 9 January 2024; published 6 February 2024)

The crystal structure, vibrational spectra, and magnetic structure of quasi-two-dimensional layered van der Waals material $MnPS_3$ were studied using x-ray diffraction and Raman spectroscopy at high pressures up to 28 GPa, and neutron diffraction up to 3.6 GPa, respectively. A structural phase transition between two monoclinic modifications of the same $C2/m$ symmetry was observed, evolving gradually in the pressure range of about 1–6 GPa. The transition is accompanied by abrupt shortening of lattice parameters, significant reduction of the monoclinic distortion, and anomalies in the pressure behavior of several Raman-mode frequencies. No more structural phase transitions were revealed in the studied pressure range. The antiferromagnetic (AFM) state with a propagation vector $k = (0, 0, 0)$ remains stable in ambient pressure and high-pressure structural phases of $MnPS_3$ at least up to 3.6 GPa. The Néel temperature increases noticeably with a pressure coefficient of $dT_N/dP = 6.7$ K/GPa, leading to modification of the dominant first-neighbor magnetic interaction exchange parameter with a relevant coefficient $dJ_1/dP \approx -0.6$ meV/GPa. This observation is in contrast to the pressure behavior of $FePS_3$, demonstrating modification of the AFM state from 2D-like to 3D-like at the similar pressure-induced structural phase transition. The different pressure response of the magnetic states of $MnPS_3$ and $FePS_3$ is analyzed in terms of competing in-plane and interplane magnetic interactions.

DOI: 10.1103/PhysRevMaterials.8.024402

I. INTRODUCTION

The recent discovery of long-range magnetic order persisting down to monolayer limit in 2D van der Waals (vdW) materials with graphenelike arrangement of their magnetic lattices has stimulated extensive research in this direction. A strong response of physical properties of vdW materials to variation of thermodynamics parameters, external actions, and chemical doping makes them a perfect platform for the search for novel physical phenomena in the 2D limit and development of advanced applications in spintronics, optospintronics, and straintronics [1,2].

One of the structurally simple model representatives of 2D van der Waals magnets is the family of transition-metal phosphorus trisulfides, MPS_3 (M = Mn, Fe, and Ni). These crystallize in the bulk monoclinic crystal structure of $C2/m$ symmetry (Fig. 1), forming layers with a honeycomb arrangement of magnetic M atoms [3]. Within each layer, linked by van der Waals forces, the P_2S_6 ligands form octahedral sulfur coordination around M atoms and P_2 pairs are arranged at the centers of the hexagons, perpendicular to the honeycomb planes. Despite the structural similarity, different types of antiferromagnetic spin arrangements in MPS_3 materials are stabilized, mediated by the type of M atoms. In $MnPS_3$, a quasi-2D Heisenberg AFM state with a propagation vector $k = (0, 0, 0)$ appears below the Néel temperature, $T_N = 78$ K. In $FePS_3$, a quasi-2D Ising AFM state with $k = (0, 1, 1/2)$ is formed below $T_N = 123$ K. In $NiPS_3$, a zigzag AFM state with $k = (0, 1, 0)$ is found below $T_N = 155$ K [4–7]. In the atomically thin forms, the antiferromagnetic order remains stable down to the bilayer of $MnPS_3$ and monolayer of $FePS_3$; in the latter case, the Néel temperature is weakly reduced to 118 K [8,9]. In $NiPS_3$, the AFM order is preserved down to the bilayer with a more pronounced reduction of T_N to about 130 K, and it is suppressed for the monolayer [10].

Recently, it was demonstrated that applying high pressure leads to the appearance of emergent physical phenomena in MPS_3 (M = Mn, Fe, and Ni) systems. In these and relevant materials, various structural phase transitions, pressure-induced metallization (M = Fe and Mn), piezochromism (M = Mn), and superconductivity ($FePSe_3$) occur [11–16]. In $FePS_3$, a strong coupling of magnetic order to structural modification was also revealed. At pressures above 2 GPa, the initial 2D-like AFM order with a propagation vector $k = (0, 1, 1/2)$ transforms to a 3D-like AFM order with a

*denk@nf.jinr.ru

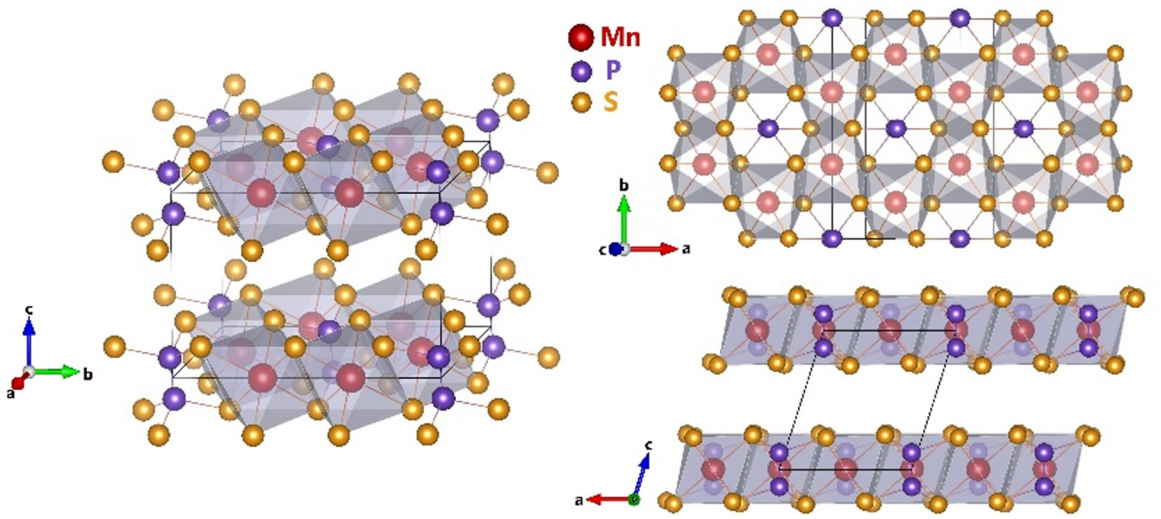

FIG. 1. The crystal structure of $MnPS_3$ [3].

propagation vector $k_1 = (0, 1, 0)$. The pressure-induced metallization leads to a melting of long-range AFM order above 13 GPa and the formation of magnetic short-range ordered state persisting above room temperature [17].

Compared with $FePS_3$, the high-pressure response of magnetic order and its relationship with structural modifications in other representatives of the MPS_3 family remains poorly explored. In this paper, we study in detail high-pressure effects on the crystal structure, magnetic structure, and vibrational properties of the $MnPS_3$ system in bulk form, employing powder x-ray diffraction and Raman spectroscopy at high pressures up to 28 GPa and powder neutron diffraction up to 3.6 GPa.

II. EXPERIMENTAL DETAILS

The x-ray powder-diffraction (XRD) experiments at high pressures up to 28 GPa were performed using the SAXS/WAXS XEUSS 3.0 system (XENOCS) and Dectris Eiger 2R 500K detector, Mo K_α radiation ($\lambda = 0.7115$ Å). A Boehler-Almax plate-type diamond-anvil cell was used in the experiments. Diamonds with culets of 300 μm were selected. Hemispherical holes with a half a culet diameter and depth of about 50 μm were made in the culet centers to improve the pressure homogeneity distribution. The sample was loaded into a hole of 150 μm diameter made in a Re gasket indented to approximately 30-μm thickness. No pressure-transmitting medium was used to avoid its interaction with the studied material. Two-dimensional XRD images were converted to one-dimensional diffraction patterns using the FIT2D program [18]. The pressure was determined using the ruby fluorescence technique at three ruby balls, one in the center of the gasket and two other close to boarders. At each ruby, accuracy of the pressure determination was on the limit of 0.1 GPa.

Raman spectra at high pressures up to 26 GPa and ambient temperature were obtained using a Confotec MR200 spectrometer (SOL Instruments) with a wavelength excitation of 532 nm from a diode-pumped solid-state laser, 1200-I/mm grating, a confocal hole of 100 μm, and a ×20 objective. The laser power was 17 mW. An absorption coefficient of $MnPS_3$ for laser excitation wavelengths in the range 488–633 cm^{-1} is relatively low (less than 1200 cm^{-1}), and the local heating effects should be negligible [19,20].

Neutron-powder diffraction measurements at pressures up to 3.6 GPa were performed at selected temperatures of 15–290 K on the DN-12 diffractometer (IBR-2 pulsed reactor, JINR, Russia) [21]. A sample with a volume of approximately 2 mm^3 was loaded into a sapphire-anvil high-pressure cell with culets of 4 mm [22]. Hemispherical holes with a diameter of 2 mm were milled at the culet centers to give a quasihydrostatic pressure distribution at the sample surface. The diffraction patterns were collected at the scattering angles of 90 ° and 45 ° with the resolution $\Delta d/d = 0.015$ and 0.022, respectively. The pressure inside the sapphire-anvil cells was measured using the ruby fluorescence technique. The pressure gradients were less than 10% concerning the average pressure value. The x-ray- and neutron-powder diffraction patterns were analyzed by the Rietveld method using the FULLPROF program [23]. The typical measurement time was about 1 h for x-ray diffraction, 1 min for Raman, and 24 h for neutron-diffraction measurements.

III. RESULTS AND DISCUSSION

A. X-ray diffraction

The x-ray diffraction patterns of $MnPS_3$, measured at selected pressures and ambient temperature, are shown in Fig. 2. At ambient conditions, they correspond to the monoclinic crystal structure of $C2/m$ symmetry. The obtained values of the lattice parameters, $a = 6.0440(5)$, $b = 10.5049(8)$, $c = 6.7866(6)$ Å and monoclinic angle $\beta = 107.65(7)^\circ$, are consistent with previous results [3]. With a pressure increase up to $P = 0.96$ GPa, extra diffraction peaks (−2 0 1) and (−1 3 2)/(1 3 2) at $2\theta = 15.4$ and 19.3 ° were observed, evidencing a structural phase transition. On further compression up to $P = 2.9$ GPa, the intensities of diffraction peaks of the ambient pressure phase were suppressed gradually, and those of the emerged high-pressure phase increased. Above 2.9 GPa, the fraction of the initial phase becomes negligible, and the pressure-induced structural phase becomes dominant. In a earlier study [15], a

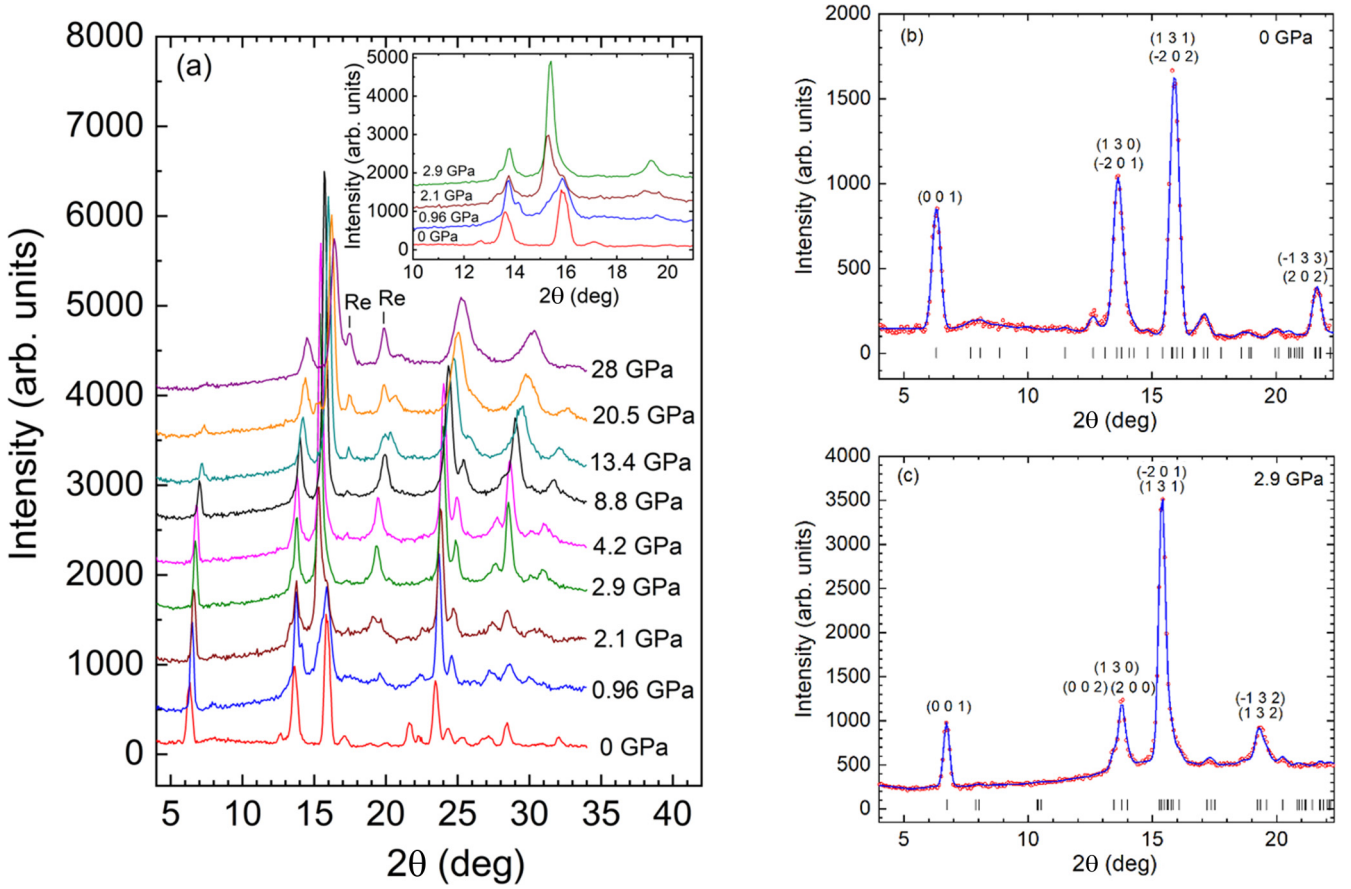

FIG. 2. XRD patterns of $MnPS_3$, measured at selected pressures (a). The inset shows the evolution of enlarged parts of XRD patterns over the structural phase transition. Sections of XRD patterns, measured at ambient pressure (b) and $P = 2.9$ GPa (c), refined by the Rietveld method. The experimental curves and calculated profiles are shown. The ticks below represent the calculated positions of the diffraction peaks.

phase coexistence in a comparable pressure range up to about 5 GPa was also found.

The Rietveld analysis shows that XRD data of the high-pressure phase may be described quite well within the monoclinic structural model of $C2/m$ symmetry but with significantly reduced lattice parameters and nearly released monoclinic distortion with the angle β now only slightly deviating from 90° (Fig. 3). A similar structural behavior was also previously observed for $FePS_3$ [24] and assumed to be a common trend for MPS_3 compounds [13]. A shear of the van der Waals planes during the phase transition results in the Mn and P atoms being located at near-equivalent geometrical positions in neighboring planes [24]. The structural parameters of initial and high-pressure phases at selected pressures are given in Table I.

The volume compressibility data of the high-pressure phase of $MnPS_3$ were fitted by the third-order Birch-Murnaghan equation of state [25]:

$$P = \tfrac{3}{2}B_0(x^{-7/3} - x^{-5/3})\left[1 + \tfrac{3}{4}(B' - 4)(x^{-2/3} - 1)\right],$$

where $x = V/V_0$ is the relative volume change, V_0 is the unit-cell volume at ambient pressure, and B_0, B' are the bulk modulus $[B_0 = -V(dP/dV)_T]$ and its pressure derivative $[B' = (dB_0/dP)_T]$. The values of $B_0 = 40(3)$ GPa and $B' = 8.0(9)$ were obtained. The bulk modulus, evaluated for the ambient pressure phase of $MnPS_3$ at pressures up to 0.5 GPa, is $B_0 = 20(5)$ GPa (with $B' = 8.0$ fixed), which is half the value of the high-pressure phase.

The lattice volume of the high-pressure phase of $MnPS_3$ demonstrates strongly preferred compression along the c axis, the direction linking vdW layers. The relevant average

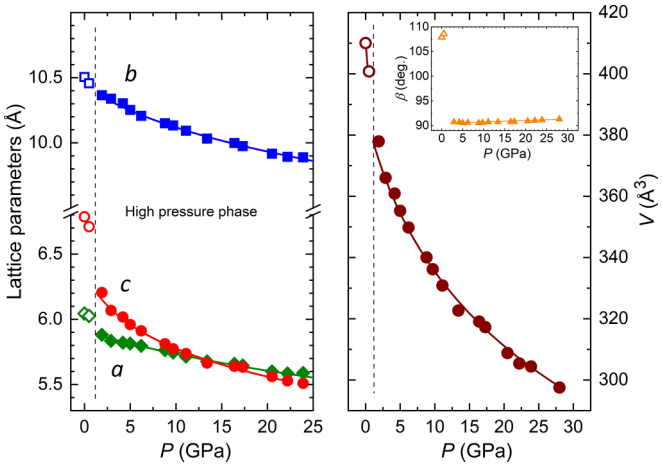

FIG. 3. The lattice parameters, unit-cell volume, and monoclinic angle (inset) of $MnPS_3$ as a function of pressure. The solid lines represent the fits based on the Birch-Murnaghan equation of state for the high-pressure phase.

TABLE I. Structural parameters of the initial and high-pressure monoclinic phases of $MnPS_3$ at selected pressures and ambient temperature. The Mn atoms are located at positions 4(*g*) (0, *y*, 0), the P and S1 atoms at positions 4(*i*) (*x*, 0, *z*), and the S2 atoms at positions 8(*j*) (*x*, *y*, *z*), space group $C2/m$. The R_p and R_{wp} factors values are also given.

P, GPa			
Lattice parameters	0	4.2	9.7
a, Å	6.0440(5)	5.8210(7)	5.7457(7)
b, Å	10.5049(8)	10.3030(9)	10.1331(9)
c, Å	6.7866(6)	6.0175(8)	5.7741(8)
β, deg.	107.65(7)	90.67(8)	90.59(8)
Atomic coordinates			
Mn: *y*	0.328(3)	0.324(4)	0.320(4)
P: *x*	0.040(6)	-0.005(6)	-0.015(6)
z	0.136(3)	0.144(4)	0.135(4)
O1: *x*	0.756(7)	0.651(8)	0.639(8)
z	0.251(3)	0.239(4)	0.239(5)
O2: *x*	0.246(4)	0.174(5)	0.153(5)
y	0.165(2)	0.164(3)	0.169(3)
z	0.252(2)	0.248(3)	0.251(3)
R_p, %	6.56	2.83	3.15
R_{wp}, %	8.21	4.01	4.12

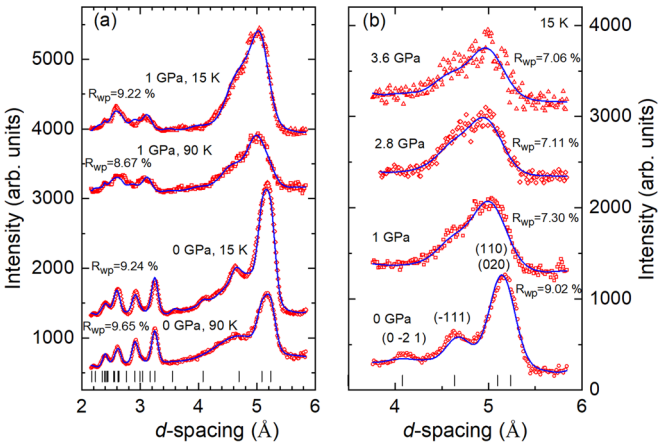

FIG. 4. The neutron-diffraction patterns of $MnPS_3$, measured at selected pressures and temperatures and fitted by the Rietveld method (a). The experimental points and calculated profiles are shown. The ticks below represent the calculated positions of the structural peaks. The magnetic contribution to sections of neutron-diffraction patterns at 15 K was obtained by subtracting data from the paramagnetic region above T_N, fitted by the Rietveld method (b). The ticks below represent the calculated positions of the peaks with the magnetic contribution.

compressibility coefficient $[k_{ai} = (-1/a_{i0})(da_i/dP)_T,\ a_i = a, b, c]$, $k_c = 0.0262\,\mathrm{GPa}^{-1}$ is about an order of magnitude larger than those for the other lattice parameters, having comparable values, $k_a = 0.0036$ and $k_b = 0.0046\,\mathrm{GPa}^{-1}$, respectively. The established character of the lattice compression is qualitatively comparable with the results of density-functional theory calculations [16]. It should be noted that the compression anisotropy along the *c* direction in $MnPS_3$ is more pronounced with respect to high-pressure phases of the vdW magnets $CrBr_3$ and Fe_3GeTe_2 having more symmetric rhombohedral and hexagonal structures. The compressibility coefficient of the *c* lattice parameter in $MnPS_3$ is about 5–7 times larger with respect to ones in Fe_3GeTe_2 and $CrBr_3$, respectively [26,27]. The difference in compressibilities of the lattice parameters lying within the vdW layers is less pronounced. The relevant coefficients for the *a* and *b* lattice parameters of $MnPS_3$, are close to those for the *a* parameter of $CrBr_3$ and about 2.7 times larger with respect to the *a* parameter of Fe_3GeTe_2.

$MnPS_3$'s monoclinic high-pressure phase remains stable in the studied pressure range up to 28 GPa. Another structural modification appears likely at higher pressures of about 29–30 GPa [12,15]. Such a structural behavior contrasts with $FePS_3$, where another structural phase transition occurs at $P \sim 14$ GPa [24].

B. Neutron diffraction

The neutron-diffraction patterns of $MnPS_3$, measured at selected pressures and temperatures, are shown in Fig. 4. At ambient pressure below the Néel temperature $T_N \approx 79(2)$ K a noticeable magnetic contribution to the intensity of the closely located peaks (0 2 0) and (1 1 0) merging into a broad peak at about 5.17 Å was observed, indicating the onset of long-range AFM order with propagation vector $k = (0,\ 0,\ 0)$. The ordered magnetic moments are oriented nearly perpendicular to the vdW (0 0 1) planes and their values evaluated at 15 K are $m = 4.3(1)\,\mu_B$, comparable with those of $4.5\,\mu_B$ found in previous studies [4,28]. In the temperature region above T_N, additional broad diffuse scattering was observed around the $(-1\ 1\ 1)$ peak located at the *d* spacing of 4.69 Å. This may occur due to the formation of a rodlike 2D lattice in the reciprocal space, related to additional magnetic phase with similar spin arrangement corresponding to the two-dimensional lattice of the vdW layers, as discussed in Ref. [28].

At high pressure of 1 GPa, a shift and redistribution of the intensity of the structural peaks initially located at ~3.2, 2.9 Å and ~2.4, 2.6 Å is observed, signaling the appearance of the structural phase transition (Fig. 4). Surprisingly, the symmetry of the long-range magnetic order remains preserved in the pressure-induced phase for the whole analyzed pressure range up to 3.6 GPa, as revealed from the Rietveld analysis of the magnetic contribution to the diffraction patterns, obtained by subtraction of the data measured in the paramagnetic region above T_N. In this procedure, the Mn atom coordinates derived from the XRD refinements were used. The observed behavior is in contrast to $FePS_3$, where a similar phase transition leads to a drastic change of zigzaglike AFM state, caused by the modification of the magnetic coupling between vdW layers from antiferromagnetic to ferromagnetic and overall magnetic structure from 2D-like to more 3D-like [17].

In order to determine a pressure dependence of the Néel temperature, the magnetic contribution to the integrated intensity of the (020)/(110) peaks (Fig. 5), normalized to that determined at 15 K, was fitted by a modified function $I_{(020)/(110)}/I_{(020)/(110)-15\,\mathrm{K}} = (1 - (T/T_N)^{\alpha})^{2\beta}$. It provides better fitting quality of experimental data for the low-temperature range in comparison with a conventional power law, corresponding to a fixed value of the parameter $\alpha = 1$. The parameter α values were found to change from 1.9(1) to

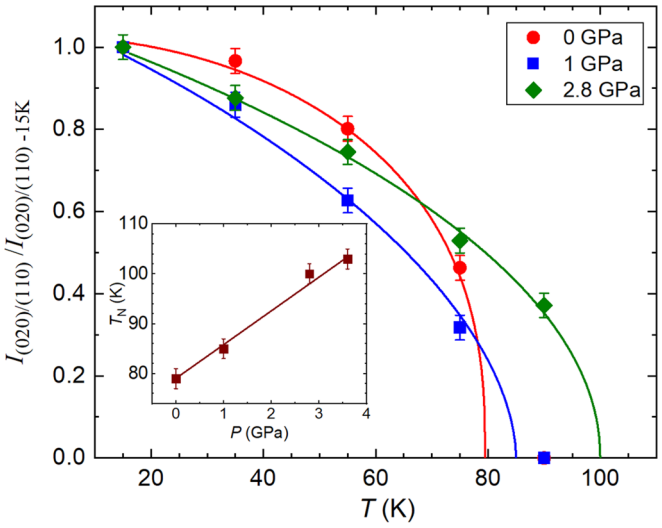

FIG. 5. Temperature dependence of the magnetic contribution to the integrated intensity of the (020)/(110) peaks at selected pressures, normalized to those determined at 15 K. The solid lines represent interpolations by functions $I_{(020)/(110)}/I_{(020)/(110)-15\,\mathrm{K}} = (1-(T/T_\mathrm{N})^{\alpha})^{2\beta}$. The pressure dependence of the Néel temperature and its linear interpolation (inset).

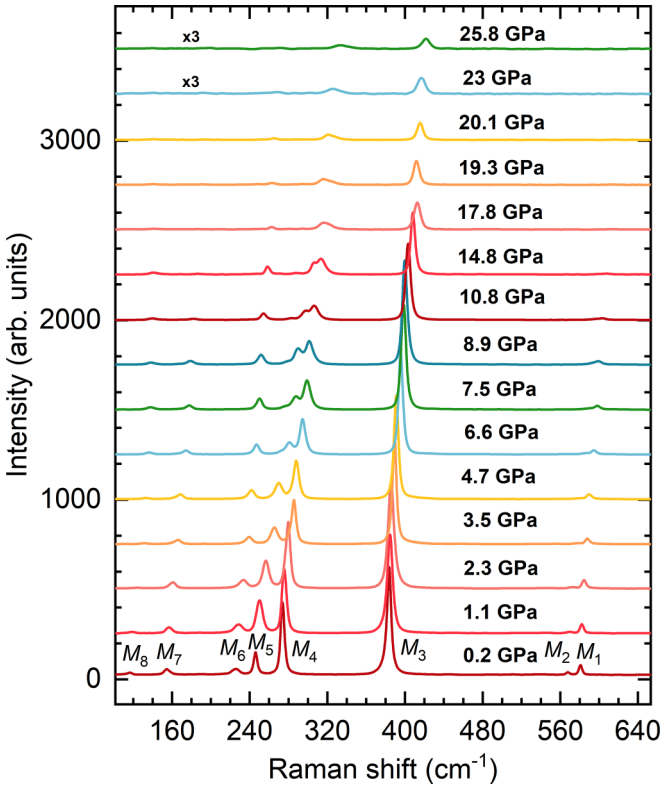

FIG. 6. The Raman spectra of $MnPS_3$, measured at high pressures up to 25.8 GPa.

1.0(1) and the critical exponent values increase slightly in the range from $\beta = 0.20(3)$ at 0 GPa to 0.24(3) at 2.8 GPa. An additional evaluation of the critical exponents using the conventional power law with $\alpha = 1$ in a more restricted temperature range down to 30 K has provided about the same values of critical exponents within the determination accuracy. The obtained β values remain comparable in the studied pressure range with one of $\beta = 0.25$, found from analysis of the (0 2 0) magnetic peak intensity, sensitive to full magnetization, in the neutron-scattering study with the single-crystalline sample of $MnPS_3$ at ambient pressure [29]. They are also close to $\beta = 0.23$, characteristic for the 2D XY model [30]. Some distinction between the β value obtained at ambient pressure in the present work with respect to Ref. [29] is likely related to use of the polycrystalline sample, providing possibility for the analysis of the merged (020)/(110) peak only based on powder neutron-diffraction data.

With a pressure increase up to 3.6 GPa, the Néel temperature increases noticeably up to 103 K with a pressure coefficient of $dT_\mathrm{N}/dP = 6.7$ K/GPa. This value is comparable with the 7.7 K/GPa obtained for the low-pressure phase of $FePS_3$ [17]. However, it is nearly half the value of $\sim$ 12 K/GPa estimated from magnetization measurements in the more restricted pressure range up to 0.9 GPa [31]. This difference is likely associated with the use of the single-crystalline sample and piston-cylinder high-pressure cell in Ref. [31], which may result in pronounced uniaxial pressure effects, if compression is performed along the c axis, linking vdW layers.

The ordered Mn magnetic moments at 15 K are reduced in magnitude by about 30% to 3.0(1) μ_B at 3.6 GPa, while their orientation with respect to the vdW (0 0 1) planes remains about the same. This observation may be associated with enhanced geometric frustration effects, mediated by competing in-plane magnetic interactions, whose balance is modified in the pressure-induced phase. The additional broadening of the magnetic contribution to the integrated intensity of the (020)/(110) peaks (Fig. 4) is likely caused by appearance of residual strains formed in the sample volume during the structural phase transition between two monoclinic modifications with noticeably different lattice parameters, superimposed on the pressure gradients (which are typically of about 10–15%).

C. Raman spectroscopy

The Raman spectra of $MnPS_3$ measured at high pressures up to 25.8 GPa are shown in Fig. 6. For the lowest pressure of 0.2 GPa, close to ambient pressure, eight vibrational modes located at 581 (M1), 568 (M2), 384 (M3), 273 (M4), 245 (M5), 226 (M6), 154 (M7), and 116 (M8) cm^{-1} were observed, in agreement with previous studies [32]. For the point group C_{2h} relevant to the monoclinic structure of $MnPS_3$ with $C2/m$ space-group symmetry of the unit cell, the Γ- point irreducible representation is $\Gamma = 16A_\mathrm{g} + 14A_\mathrm{u} + 12B_\mathrm{g} + 18B_\mathrm{u}$, where A_g and B_g modes are Raman active [33].

The observed vibrational modes were assigned according to Refs. [8,32] and presented in Table II. The metal-ion vibrations noticeably contribute to the lower-frequency modes (M6–M8), while higher-frequency modes (M1–M5) involve mainly vibrations of the P_2S_6 molecular groups. In particular, the M1 mode is associated with P–P bond stretching, the M3 mode with P–S bond symmetric stretching, and the M5 mode with movements of the chalcogen planes in opposite directions to each other, providing modulation of the van der Waals gap [32,33].

The frequencies of all the observed modes increase upon lattice compression (Fig. 7). The pressure behaviors of

TABLE II. The assignment of the observed Raman modes of $MnPS_3$, pressure coefficients, and mode-Grüneisen parameters γ_i calculated for different pressure ranges. The mode-Grüneisen parameters γ_i are determined as $\gamma_i = B_0/[v_i(dv_i/dP)_T]$, where B_0 is the bulk modulus.

Raman mode	v_0 (cm^{-1})	dv_i/dP (cm^{-1}/GPa)		γ_i	
M_1	580	2.33 $P < 6$ GPa	1.58 $P > 6$ GPa	0.08 $P < 6$ GPa	0.11 $P > 6$ GPa
		$P < 12$ GPa	$P > 12$ GPa	$P < 12$ GPa	$P > 12$ GPa
M_2	567.9	2.76	–	0.09	–
M_3	383.8	1.94	1.12	0.1	0.11
M_4	273.6	3.2	1.47	0.23	0.2
		$P < 6$ GPa	$P > 6$ GPa	$P < 6$ GPa	$P > 6$ GPa
M_5	245.7	5.56	2.47	0.45	0.36
M_6	225.9	3.35	1.2	0.29	0.2
M_7	154.6	3.15	1.29	0.41	0.31
M_8	116.6	3.3	0.28	0.57	0.08
M_9	275.9	–	1.63	–	0.24

the lower-frequency M5–M8 modes demonstrate anomalies caused by a change of pressure coefficients (their values dv_i/dP along with the mode-Grüneisen parameters are listed in Table II) at $P \sim 6$ GPa. The above-mentioned modes involve both P_2S_6 groups' and Mn atoms' vibrations, rearrangement of which in the crystal lattice during the phase transition results in modification of their pressure dependences due to different compression properties of the initial and pressure-induced phases. As the transition evolves over a phase coexistence range, this effect becomes well visible at completion of the transition at $P \sim 6$ GPa. In contrast, high-frequency modes are associated with the P_2S_6 molecular group vibrations only, geometry of which is not affected by the phase transition, providing absence of well-detectable anomalies in their pressure behaviors.

Above $P = 6$ GPa, an additional weak mode (M9) at 275 cm^{-1} was also detected. Its appearance may be related to splitting the M4 mode into A_g and B_g components due to structural modification at the phase transition. Indeed, the mode-Grüneisen parameters of these modes (Table II) are very close, supporting this conclusion.

The mode-Grüneisen parameters associated with intramolecular vibrations of the P_2S_6 molecular groups (M1, M3, and M4) remain about the same in the pressure-induced phase, while those involving vibrations of metal ions (M6–M8) or vibrations of chalcogen atoms in neighboring vdW planes (M5) decrease noticeably (Table II). The most pronounced reduction of the γ value is found for the M8 mode, involving in-plane vibrations of the Mn atoms.

At pressures around 12–15 GPa, a merging of the M1 and M2 modes and less-pronounced changes in the pressure slope of the M3 and M4 modes were revealed. In this pressure region, the *a*- and *c*-lattice parameters become close (Fig. 2) and their relationship changes from $a > c$ to $a < c$. The structural rearrangements within the monoclinic high-pressure phase associated with the lattice compression anisotropy may be responsible for these effects. Previously, such effects were ascribed to a possible structural phase transition in $MnPS_3$, resulting in the change of the lattice symmetry to trigonal $P\bar{3}1m$ [14], as in $FePS_3$ at $P \sim 14$ GPa [24]. However, this transition in $FePS_3$ results in a huge interplanar distance collapse by about 15% [17], which could be easily detected by the abrupt shift of the (0 0 1) diffraction peak and collapse of the *c*-lattice parameter. The absence of an abrupt shift in (0 0 1) peak position located at $2\theta \approx 6.3^\circ$ as well as other qualitative changes at 12–15 GPa in our XRD data and

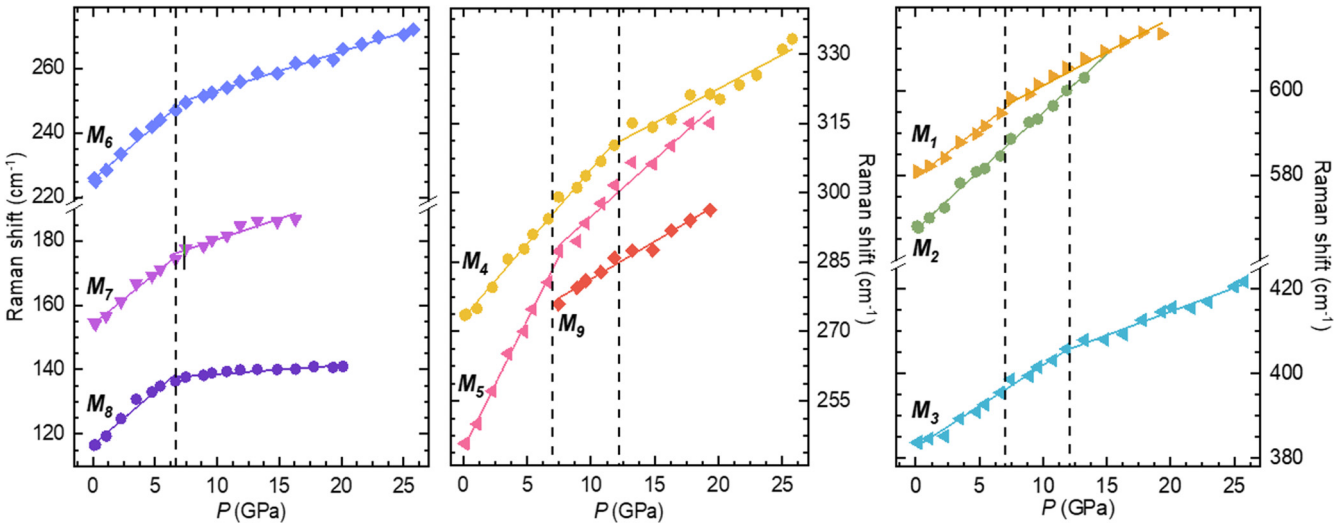

FIG. 7. Pressure dependencies of the observed Raman-mode frequencies of $MnPS_3$. Solid lines represent linear fits to experimental data.

anomalies in pressure behavior of lattice parameters allow us to exclude this scenario for $MnPS_3$. Moreover, at the pressure-induced monoclinic-trigonal phase transition in $FePS_3$, abrupt shifts of particular modes' frequencies to higher values and several extra modes appeared [34,35]. This contrasts with the observed pressure behavior of Raman spectra of $MnPS_3$. All these findings allow us to exclude the scenario of the monoclinic-trigonal phase transition in $MnPS_3$ at 12–15 GPa and associate the observed effects with the structural rearrangements within the high-pressure monoclinic phase. It should be noted that another structural phase transition with a significant volume collapse, accompanied by the semiconductor-metal transition, was found in $MnPS_3$ at higher pressures of about 29–30 GPa [12,15]. This suggests that the trigonal phase in $MnPS_3$ is formed at $P \sim 30$ GPa, which is beyond the scope of the present study.

D. Discussion

The pressure-induced structural phase transition of the same nature results in a drastically different response of the magnetic state of $MnPS_3$ compared to $FePS_3$. In the MPS_3 systems, long-range magnetic order is formed by a competing balance of first- (J_1), second- (J_2), and third- (J_3) nearest-neighbor magnetic interactions within the vdW planes and much weaker interplane (J_i) interactions [36,37]. For $MnPS_3$, exchange constants for all the in-plane interactions are negative, and the first-neighbor interaction is the strongest one, $J_1 = -0.77$, $J_2 = -0.07$, and $J_3 = -0.18$ meV, while $J_i = 0.0019$ meV is positive [29]. Accordingly, an AFM state with propagation vector $q = (0,\ 0,\ 0)$ is formed, with AFM coupling of the nearest-neighboring Mn spins within the vdW planes and FM coupling of neighboring vdW planes along the c axis. Upon lattice compression, the symmetry of the magnetic state is preserved, and the Néel temperature increases with a relatively large pressure coefficient of $dT_N/dP = 6.7$ K/GPa. This implies that the leading first-neighbor AFM interaction strength increases significantly while the interplane magnetic interaction remains FM. In the mean-field approach [38], neglecting the weakest interplane magnetic interaction, the relationship between T_N and the in-plane exchange parameters is

$$T_N = S(S+1)(-3J_1 - 6J_2 - 3J_3)/3k_B,$$

where $S = 5/2$ is the spin of Mn^{2+} ions and k_B is the Boltzmann constant.

For $MnPS_3$, J_2 and J_3 exchange constants are much smaller in magnitude with respect to J_1. Neglecting their contribution, one may evaluate the pressure coefficient for the leading first-neighbor exchange constant J_1 as $dJ_1/dP \approx -0.6$ meV/GPa.

For $FePS_3$, the exchange constant of the first-neighbor in-plane interaction is positive, while those of the second- and third-neighbor in-plane interactions, as well as the interplanar one, are negative, $J_1 = 1.46$, $J_2 = -0.04$, $J_3 = -0.96$ meV, and $J_i = -0.007$ meV [36]. Due to comparable magnitudes and opposite sign of J_1 and J_3, and negative J_i, a more complex zigzaglike AFM state with the antiparallel coupling of Fe spins between the neighboring vdW planes along the c axis with a propagation vector $k = (0,\ 1,\ 1/2)$ is formed. In the pressure-induced monoclinic phase, long-range magnetic order is modified from 2D-like to 3D-like with a propagation vector $k_1 = (0,\ 1,\ 0)$ and parallel spin arrangement of Mn^{2+} ions in the neighboring planes along the c axis [17]. This implies that high pressure modifies the sign of the interplanar exchange constant J_i from negative to positive. A larger value of the pressure coefficient $dT_N/dP = 7.7$ K/GPa for $FePS_3$ reflects a more noticeable contribution from the third-nearest in-plane magnetic exchange interaction, more pronounced than in $MnPS_3$.

IV. CONCLUSIONS

The obtained results have provided important insights into the high-pressure behavior of the structural and magnetic states of quasi-two-dimensional layered van der Waals material $MnPS_3$. A gradual structural phase transition to a pressure-induced monoclinic phase with a released monoclinic distortion and significantly reduced lattice parameters evolves in the pressure range of ~1–6 GPa, as evidenced by the XRD and Raman spectroscopy data. In the phase transition region, anomalies in the pressure behavior of several Raman modes were observed. There was no evidence for additional phase transitions in the studied pressure range up to 28 GPa.

The AFM magnetic state with a propagation vector $k = (0, 0, 0)$ remains stable in $MnPS_3$ at high pressures, at least up to 3.6 GPa, and the Néel temperature increases noticeably with a pressure coefficient of $dT_N/dP = 6.7$ K/GPa, resulting in the relevant modification of the exchange parameter of the leading first-neighbor magnetic interaction with a pressure coefficient $dJ_1/dP \approx -0.6$ meV/GPa. The contrasting pressure behavior of the magnetic state of $MnPS_3$ with respect to $FePS_3$ is caused mainly by different signs of interplane magnetic interaction exchange constant at ambient pressure, which remains positive in the case of $MnPS_3$, and changes from negative to positive under pressure in $FePS_3$. The established relationships between structural and magnetic pressure behaviors of $MnPS_3$ and related MPS_3 materials are important for further development of applications based on pressure and strain response of their functional properties as elements of photoelectronic, spintronic, and straintronic devices.

ACKNOWLEDGMENT

Work at SNU was funded by the Leading Researcher Program of the National Research Foundation of Korea (Grant No. 2020R1A3B2079375). This work was also supported by the Vietnam National Foundation for Science and Technology Development (NAFOSTED) under Grant No. 103.02-2021.70.

[1] K. S. Burch, D. Mandrus, and J. G. Park, Magnetism in two-dimensional van der Waals materials, Nature (London) **563**, 47 (2018).

[2] M. Gibertini, M. Koperski, A. F. Morpurgo, and K. S. Novoselov, Magnetic 2D materials and heterostructures, Nat. Nanotechnol. **14**, 408 (2019).

[3] G. Ouvrard, R. Brec, and J. Rouxel, Structural determination of some MPS_3 layered phases (M = Mn, Fe, Co, Ni and Cd), Mater. Res. Bull. **20**, 1181 (1985).

[4] K. Kurosawa, S. Saito, and Y. Yamaguchi, Neutron diffraction study on $MnPS_3$ and $FePS_3$, J. Phys. Soc. Jpn. **52**, 3919 (1983).

[5] P. A. Joy and S. Vasudevan, Magnetism in the layered transition-metal thiophosphates MPS_3, (M = Mn, Fe, and Ni), Phys. Rev. B **46**, 5425 (1992).

[6] D. Lançon, H. C. Walker, E. Ressouche, B. Ouladdiaf, K. C. Rule, G. J. McIntyre, T. J. Hicks, H. M. Rønnow, and A. R. Wildes, Magnetic structure and magnon dynamics of the quasi-two-dimensional antiferromagnet $FePS_3$, Phys. Rev. B **94**, 214407 (2016).

[7] A. R. Wildes, V. Simonet, E. Ressouche, G. J. McIntyre, M. Avdeev, E. Suard, S. A. J. Kimber, D. Lançon, G. Pepe, B. Moubaraki, and T. J. Hicks, Magnetic structure of the quasi-two-dimensional antiferromagnet $NiPS_3$, Phys. Rev. B **92**, 224408 (2015).

[8] K. Kim, S. Y. Lim, J. Kim, J.-U. Lee, S. Lee, P. Kim, K. Park, S. Son, C.-H. Park, J.-G. Park, and H. Cheong, Antiferromagnetic ordering in van der Waals two dimensional magnetic material $MnPS_3$ probed by Raman spectroscopy, 2D Mater. **6**, 041001 (2019).

[9] J.-U. Lee, S. Lee, J. H. Ryoo, S. Kang, T. Y. Kim, P. Kim, C.-H. Park, J.-G. Park, and H. Cheong, Ising-type magnetic ordering in atomically thin $FePS_3$, Nano Lett. **16**, 7433 (2016).

[10] K. Kim, S. Y. Lim, J.-U. Lee, S. Lee, T. Y. Kim, K. Park, G. S. Jeon, C.-H. Park, J.-G. Park, and H. Cheong, Suppression of magnetic ordering in XXZ-type antiferromagnetic monolayer $NiPS_3$, Nat. Commun. **10**, 345 (2019).

[11] Y. Wang, J. Ying, Z. Zhou, J. Sun, T. Wen, Y. Zhou, N. Li, Q. Zhang, F. Han, Y. Xiao, P. Chow, W. Yang, V. V. Struzhkin, Y. Zhao, and H. K. Mao, Emergent superconductivity in an iron-based honeycomb lattice initiated by pressure-driven spin-crossover, Nat. Commun. **9**, 1914 (2018).

[12] Y. Wang, Z. Zhou, T. Wen, Y. Zhou, N. Li, F. Han, Y. Xiao, P. Chow, J. Sun, M. Pravica, A. L. Cornelius, W. Yang, and Y. Zhao, Pressure-driven cooperative spin-crossover, large-volume collapse, and semiconductor-to-metal transition in manganese(II) honeycomb lattices, J. Am. Chem. Soc. **138**, 15751 (2016).

[13] M. J. Coak, D. M. Jarvis, H. Hamidov, C. R. S. Haines, P. L. Alireza, C. Liu, S. Son, I. Hwang, G. I. Lampronti, D. Daisenberger, P. Nahai-Williamson, A. R. Wildes, S. S. Saxena, and J.-G. Park, Tuning dimensionality in van-der-Waals antiferromagnetic Mott insulators $TMPS_3$, J. Phys.: Condens. Matter **32**, 124003 (2020).

[14] N. C. Harms, H.-S. Kim, A. J. Clune, K. A. Smith, K. R. O'Neal, A. V. Haglund, D. G. Mandrus, Z. Liu, K. Haule, D. Vanderbilt, and J. L. Musfeldt, Piezochromism in the magnetic chalcogenide $MnPS_3$, npj Quantum Mater. **5**, 56 (2020).

[15] D. M. Jarvis, Structural and Magnetic Phases in Pressure-Tuned Quantum Materials, Ph.D. Thesis, University of Cambridge, 2020.

[16] H.-S. Kim, K. Haule, and D. Vanderbilt, Mott metal-insulator transitions in pressurized layered trichalcogenides, Phys. Rev. Lett. **123**, 236401 (2019).

[17] M. J. Coak, D. M. Jarvis, H. Hamidov, A. R. Wildes, J. A. M. Paddison, C. Liu, C. R. S. Haines, N. T. Dang, S. E. Kichanov, B. N. Savenko, S. Lee, M. Kratochvilova, S. Klotz, T. Hansen, D. P. Kozlenko, J.-G. Park, and S. S. Saxena, Evolution of magnetic order in van der Waals antiferromagnet $FePS_3$ through insulator-metal transition, Phys. Rev. X **11**, 011024 (2021).

[18] A. P. Hammersley, S. O. Svensson, M. Hanfland, A. N. Fitch, and D. Hausermann, Two-dimensional detector software: From real detector to idealised image or two-theta scan, High Press. Res. **14**, 235 (1996).

[19] F. Kargar, E. A. Coleman, S. Ghosh, J. Lee, M. J. Gomez, Y. Liu, A. S. Magana, Z. Barani, A. Mohammadzadeh, B. Debnath, R. B. Wilson, R. K. Lake, and A. A. Balandin, Phonon and thermal properties of quasi-two-dimensional $FePS_3$ and $MnPS_3$ antiferromagnetic semiconductors, ACS Nano **14**, 2424 (2020).

[20] R. Brec, D. M. Schleich, G. Ouvrard, A. Louisy, and J. Rouxel, Physical properties of lithium intercalation compounds of the layered transition-metal chalcogenophosphites, Inorg. Chem. **18**, 1814 (1979).

[21] V. L. Aksenov, A. M. Balagurov, V. P. Glazkov, D. P. Kozlenko, I. V. Naumov, B. N. Savenko, D. V. Sheptyakov, V. A. Somenkov, A. P. Bulkin, V. A. Kudryashev, and V. A. Trounov, DN-12 time-of-flight high-pressure neutron spectrometer for investigation of microsamples, Physica B **265**, 258 (1999).

[22] D. P. Kozlenko, S. E. Kichanov, E. V. Lukin, and B. N. Savenko, High pressure neutron diffraction studies of the crystal and magnetic structure of materials at the pulsed reactor IBR-2: Current opprtunities and prospects, Crystallogr. Rep. **66**, 303 (2021).

[23] J. Rodríguez-Carvajal, Recent advances in magnetic structure determination by neutron powder diffraction, Physica B **192**, 55 (1993).

[24] C. R. S. Haines, M. J. Coak, A. R. Wildes, G. I. Lampronti, C. Liu, P. Nahai-Williamson, H. Hamidov, D. Daisenberger, and S. S. Saxena, Pressure-induced electronic and structural phase evolution in the van der Waals compound $FePS_3$, Phys. Rev. Lett. **121**, 266801 (2018).

[25] F. J. Birch, Equation of state and thermodynamic parameters of NaCl to 300 kbar in the high-temperature domain, J. Geophys. Res. **91**, 4949 (1986).

[26] N. T. Dang, D. P. Kozlenko, O. N. Lis, S. E. Kichanov, E. V. Lukin, N. O. Golosova, B. N. Savenko, D.-L. Duong, T.-L. Phan, T. A. Tran, and M. H. Phan, High pressure-driven magnetic disorder and structural transformation in Fe_3GeTe_2: Emergence of a magnetic quantum critical point, Adv. Sci. **10**, 2206842 (2023).

[27] O. N. Lis, D. P. Kozlenko, S. E. Kichanov, E. V. Lukin, I. Yu Zel, and B. N. Savenko, Structural, magnetic and vibrational properties of van der Waals ferromagnet $CrBr_3$ at high pressure, Materials **16**, 454 (2023).

[28] A. R. Wildes, S. J. Kennedy and T. J. Hicks, True two-dimensional magnetic ordering in $MnPS_3$, J. Phys.: Condens. Matter **6**, L335 (1994).

[29] A. R. Wildes, B. Roessli, B. Lebech, and K. W. Godfrey, Spin waves and the critical behaviour of the magnetization in $MnPS_3$, J. Phys.: Condens. Matter **10**, 6417 (1998).

[30] S. T. Bramwell and P. C. W. Holdsworth, Magnetization and universal sub-critical behaviour in two-dimensional XY magnets, J. Phys.: Condens. Matter **5**, L53 (1993).

[31] W. Toyoshima, T. Masubuchi, T. Watanabe, K. Takase, K. Matsubayashi, Y. Uwatoko, and Y. Takano, Pressure dependence of the magnetic properties of $MnPS_3$, J. Phys.: Conf. Ser. **150**, 042215 (2009).

[32] M. Bernasconi, G. L. Marra, G. Benedek, L. Miglio, M. Jouanne, C. Julien, M. Scagliotti, and M. Balkanski, Lattice dynamics of layered MPX_3 (M= Mn,Fe,Ni,Zn; X= S,Se) compounds, Phys. Rev. B **38**, 12089 (1988).

[33] M. Scagliotti, M. Jouanne, M. Balkanski, G. Ouvrard, and G. Benedek, Raman scattering in antiferromagnetic $FePS_3$ and $FePSe_3$ crystals, Phys. Rev. B **35**, 7097 (1987).

[34] S. Das, S. Chaturvedi, D. Tripathy, S. Grover, R. Singh, D. V. S. Muthu, S. Sampath, U. V. Waghmare, and A. K. Sood, Raman and first-principles study of the pressure-induced Mott-insulator to metal transition in bulk $FePS_3$, J. Phys. Chem. Solids **164**, 110607 (2022).

[35] H. Zeng, T. Ye, P. Cheng, D. Yao, and J. Ding, Raman spectroscopy investigation on the pressure-induced structural and magnetic phase transition in two-dimensional antiferromagnet $FePS_3$, Chin. Phys. B **31**, 056109 (2022).

[36] D. Lançon, R. A. Ewings, T. Guidi, F. Formisano, and A. R. Wildes, Magnetic exchange parameters and anisotropy of the quasi-two-dimensional antiferromagnet $NiPS_3$, Phys. Rev. B **98**, 134414 (2018).

[37] G. L. Flem, R. Brec, G. Ouvard, A. Louisy, and P. Segransan, Magnetic interactions in the layer compounds MPX_3 (M = Mn, Fe, Ni; X = S, Se), J. Phys. Chem. Solids **43**, 455 (1982).

[38] R. Basnet, K. M. Kotur, M. Rybak, C. Stephenson, S. Bishop, C. Autieri, M. Birowska, and J. Hu, Controlling magnetic exchange and anisotropy by nonmagnetic ligand substitution in layered MPX_3 (M = Ni, Mn; X = S, Se), Phys. Rev. Res. **4**, 023256 (2022).